Journal of Hazardous Materials 196 (2011) 302–310

Contents lists available at SciVerse ScienceDirect

Journal of Hazardous Materials

journal homepage: www.elsevier.com/locate/jhazmat

Partitioning behavior and stabilization of hydrophobically coated HfO_2, ZrO_2 and $Hf_xZr_{1-x}O_2$ nanoparticles with natural organic matter reveal differences dependent on crystal structure

Divina A. Navarro[1], Sean W. Depner, David F. Watson, Diana S. Aga*, Sarbajit Banerjee**

Department of Chemistry, University at Buffalo, State University of New York, Buffalo, NY 14260-3000, USA

ARTICLE INFO

Article history:
Received 11 April 2011
Received in revised form 7 September 2011
Accepted 8 September 2011
Available online 14 September 2011

Keywords:
Twin-metal oxides
Natural organic matter
Phase transfer
Nanoparticle structure
Environmental mobility
Colloidal interactions

ABSTRACT

The interactions of engineered nanomaterials with natural organic matter (NOM) exert a profound influence on the mobilities of the former in the environment. However, the influence of specific nanomaterial structural characteristics on the partitioning and colloidal stabilization of engineered nanomaterials in various ecological compartments remains underexplored. Herein, we present a systematic study of the interactions of humic acid (HA, as a model for NOM) with monodisperse, well-characterized, ligand-passivated HfO_2, ZrO_2, and solid-solution $Hf_xZr_{1-x}O_2$ nanoparticles (NPs). We note that mixing with HA induces the almost complete phase transfer of hydrophobically coated monoclinic metal oxide (MO) NPs from hexane to water. Furthermore, HA is seen to impart appreciable colloidal stabilization to the NPs in the aqueous phase. In contrast, phase transfer and aqueous-phase colloidal stabilization has not been observed for tetragonal MO-NPs. A mechanistic model for the phase transfer and aqueous dispersal of MO-NPs is proposed on the basis of evidence from transmission electron microscopy, ζ-potential measurements, dynamic light scattering, Raman and infrared spectroscopies, elemental analysis, and systematic experiments on a closely related set of MO-NPs with varying composition and crystal structure. The data indicate the synergistic role of over-coating (micellar), ligand substitution (coordinative), and electrostatic processes wherein HA acts both as an amphiphilic molecule and a charged chelating ligand. The strong observed preference for the phase transfer of monoclinic instead of tetragonal NPs indicates the importance of the preferential binding of HA to specific crystallographic facets and suggests the possibility of being able to design NPs to minimize their mobilities in the aquatic environment.

1. Introduction

The imminent large-scale commercialization of engineered nanomaterials (ENMs) has raised concerns regarding their potential environmental impact [1–4]. Some preliminary data are starting to become available regarding the toxicity of ENMs at the sub-cellular, cellular, and organism levels [5–8]. Among these materials, transition metal oxide (MO)-based nanoparticles (NPs) are finding various applications as nanoceramic fillers within composite materials, magnetic recording media, catalyst supports, and sensing elements [9]. Most notably, HfO_2 and ZrO_2 NPs have found widespread applications in optical and protective coating technologies due to their thermal stability and high dielectric constants [10]. In particular, these materials are promising alternatives to SiO_2 as gate dielectric layers for flexible electronics [11–13]. The underlying premise of flexible electronics has been affordability and ubiquitous availability on standard media such as paper and cloth. Consequently, with increasing commercial production, consumer use, and end-user disposal, the release of these NPs to different environmental compartments (especially water and soil) is inevitable.

In particular, waste generated during manufacturing processes will have a high concentration of NPs. Although, the likelihood of the release of MO NPs affixed within device structures is not high, environmental discharge may occur over a protracted period of time, especially as a result of material abuse and towards the end of product life. Given the low proposed cost of flexible electronic devices and lack of specifications regarding disposal outlined by manufacturers, several of these materials may eventually enter landfills and run-off streams through household waste disposal. A systematic understanding of partitioning behavior, potential mobilities, and persistence of MO NPs is thus necessary for

* Corresponding author. Tel.: +1 716 645 4220; fax: +1 716 645 6963.
** Corresponding author. Tel.: +1 716 645 4140; fax: +1 716 645 6963.
E-mail addresses: dianaaga@buffalo.edu (D.S. Aga), sb244@buffalo.edu (S. Banerjee).
[1] Current address: CSIRO Land and Water, Advanced Materials Transformational Capability Platform, Nanosafety, Biogeochemistry Program, Waite Campus, Waite Rd, SA 5155, Australia.

0304-3894/$ – see front matter © 2011 Elsevier B.V. All rights reserved.
doi:10.1016/j.jhazmat.2011.09.028

evaluating potential ecological hazards and framing informed policy [1].

Up till now, the environmental fate and transport of ENMs have been characterized under different environmental conditions (i.e., pH, ionic strength, organic colloids, etc.). The influence of natural organic matter (NOM) on NP behavior in the environment has been emphasized in many studies because of the ubiquity of the former in aquatic and soil environments. Indeed, the nature and amount of NOM in water have been demonstrated (both theoretically and experimentally) to affect the stability and bioavailability of a variety of NPs [14–20]. In many cases, the stability of NPs in aqueous suspension is often attributed to the adsorption of NOM. However, these reports only tend to deem adsorption as a primary mechanism for interaction based on indirect measures such as transmission electron microscopy (TEM), ζ-potential, and light scattering, which are somewhat limited in characterizing surface-related interactions.

An evaluation of the chemical structure of NOM and colloidal MO-NPs suggests several distinctive processes that can facilitate the stabilization of NPs in the aqueous phase. NOM has a highly complex molecular structure, which includes a skeleton of alkyl and aromatic units with pendant functional groups including carboxylic acid, phenolic hydroxyl, and quinone moieties [21–23]. MO-NPs, on the other hand, comprise an inorganic core passivated by a layer of organic ligands [11,24]. The crystalline core can adopt different crystal structures depending on the specifics of composition and stoichiometry (HfO_2 and ZrO_2 NPs adopt monoclinic and tetragonal crystal structures, respectively) [25,11]. The intrinsic morphological, energetic, and surface chemical properties of NOM enable them to interact with and stabilize different species via amphiphilic and metal-chelating processes. In addition to the organic ligands that surround the crystalline core, MO-NPs also have highly reactive surfaces (edge and corner sites) that greatly influence their behavior and reactivity [26–28]. While these structural and surface characteristics are well known to be important in surface science, these details have typically been overlooked in many fate and transport studies.

Very few studies thus far have focused on the transformations of ligand-passivated NPs prepared by hot colloidal chemistry methods upon interactions with NOM. Such ligand-capped NPs are indeed likely to be the mainstay of most nanoscience-enabled technologies [29–32]. Herein, we describe systematic studies on the interaction of ligand-passivated HfO_2, ZrO_2, and $Hf_xZr_{1-x}O_2$ NPs with Suwannee River humic acid (HA) as a model for NOM. The following topics have been addressed in this work: (1) the partitioning of hydrophobically coated MO-NPs, with or without HA, in the aqueous phase; (2) examination of interactions that enable HA to colloidally stabilize MO-NPs (i.e., electrostatic, coordinative, and dispersive interactions); and (3) the importance of both NP surface (crystal structure: monoclinic or tetragonal) and passivating ligands (surface coating: tri-*n*-octylphosphine oxide (TOPO)) on the stabilization of NPs by HA in water; TOPO is a ubiquitous ligand in nanoscience and is commonly used in hot colloidal synthesis. This study provides a mechanistic report of the aqueous-phase stabilization of different types of hydrophobically coated MO-NPs with and without HA. In particular, we have attempted to directly characterize processes that govern the adsorption and agglomeration of MO-NPs with HA.

2. Experimental

2.1. Materials

The monoclinic (m-) HfO_2 and $Hf_{0.37}Zr_{0.63}O_2$, and tetragonal (t-) ZrO_2 and $Hf_{0.37}Zr_{0.63}O_2$ NP powders used in these experiments were synthesized by the non-hydrolytic sol–gel condensation of metal alkoxides with metal halides using TOPO (Strem Chemicals, MA, USA) as the coordinating ligand [11]. This synthetic approach provides monodispersity and excellent control over crystal structure, size, and stoichiometry. The TOPO ligand coordinates to surficial atoms, completing the coordination shell for undercoordinated metal sites, and thereby serving as a passivating coating. The use of monodisperse systems provides standardization required for careful mechanistic studies and precludes obscuration from polydispersities in particle size, surface capping, and crystal structure, which would substantially complicate studies of MO-NPs with NOM. All MO-NP powders were readily dispersible in hexane. Approximately 500–1000 mg/L NP suspensions were prepared and used for the phase transfer experiments; these concentrations were chosen for ease in detection of NPs. No consensus has yet emerged on what constitutes an environmentally realistic concentration of MO NPs. The use of the said concentrations allows us to deploy standard microscopy and spectroscopy tools for elucidation of the nature of NP–NOM interactions and indeed such interactions are likely to persist even at low concentrations. For aqueous solubility tests, NP powders were dispersed in water.

Suwannee River HA (SRHA-II) standard was purchased from International Humic Substances Society (St. Paul, MN, USA). The use of well-characterized SRHA-II also enables standardization, articulated at various international workshops as an urgent goal for establishing generalizable means of evaluation of ENM fate and transport. Given our primary goal of elucidating the mechanistic basis for ENM phase transfer, the use of well-characterized NOM acquires paramount importance.

For Hf/Zr analysis, metal standards (fluoride-soluble metals) and Aristar Ultra grade concentrated HF and HNO_3 from BDH Chemicals (West Chester, PA, USA) were used in standard preparation and acid digestions, respectively. Deionized (DI) water from a Barnstead NANOpure (USA) water system was used to prepare all aqueous solutions (resistivity = 18.2 MΩ/cm).

2.2. Phase transfer experiments

A 5-mL aliquot of the MO-NP suspension (in hexane) was mixed with 5 mL of 20 mg/L HA in DI water (pH ∼ 4.4) in a clear vial. This experimental construct is referred to as a "phase transfer set-up". A 20 mg/L HA solution contains 12.5 mg/L dissolved organic carbon that is within levels typical of natural waters (0.1–200 mg/L) [33]. The low natural pH used here is also representative of the low pH of the Suwanee River where the HA was sampled. Similar conditions were used in our previous work on CdSe QDs [30,31]. Phase transfer set-ups were also prepared in DI water (no HA) to serve as controls. Our intention was to study the interactions of MO-NPs with analogs of actual environmental samples, containing controlled concentrations of HA. In between measurements, each set-up was protected from light using Al foil, and was stirred continuously at room temperature using a rocking platform shaker to stimulate natural mixing and fluid diffusion processes. Mixing was performed for 15 days (∼2 weeks). For metal analyses, individual phase transfer set-ups (0, 1, 3, 5, 10, and 15 days) were prepared; this avoids sampling errors due to interfacial aggregation (i.e., removal of flocculated aggregates as the volume of solution is reduced).

2.3. Analysis and instrumentation

Qualitative and quantitative analyses were performed using ζ-potential measurements, dynamic light scattering (DLS), TEM, Raman and Fourier transform infrared (FTIR) spectroscopies and inductively coupled plasma mass spectrometry (ICP-MS).

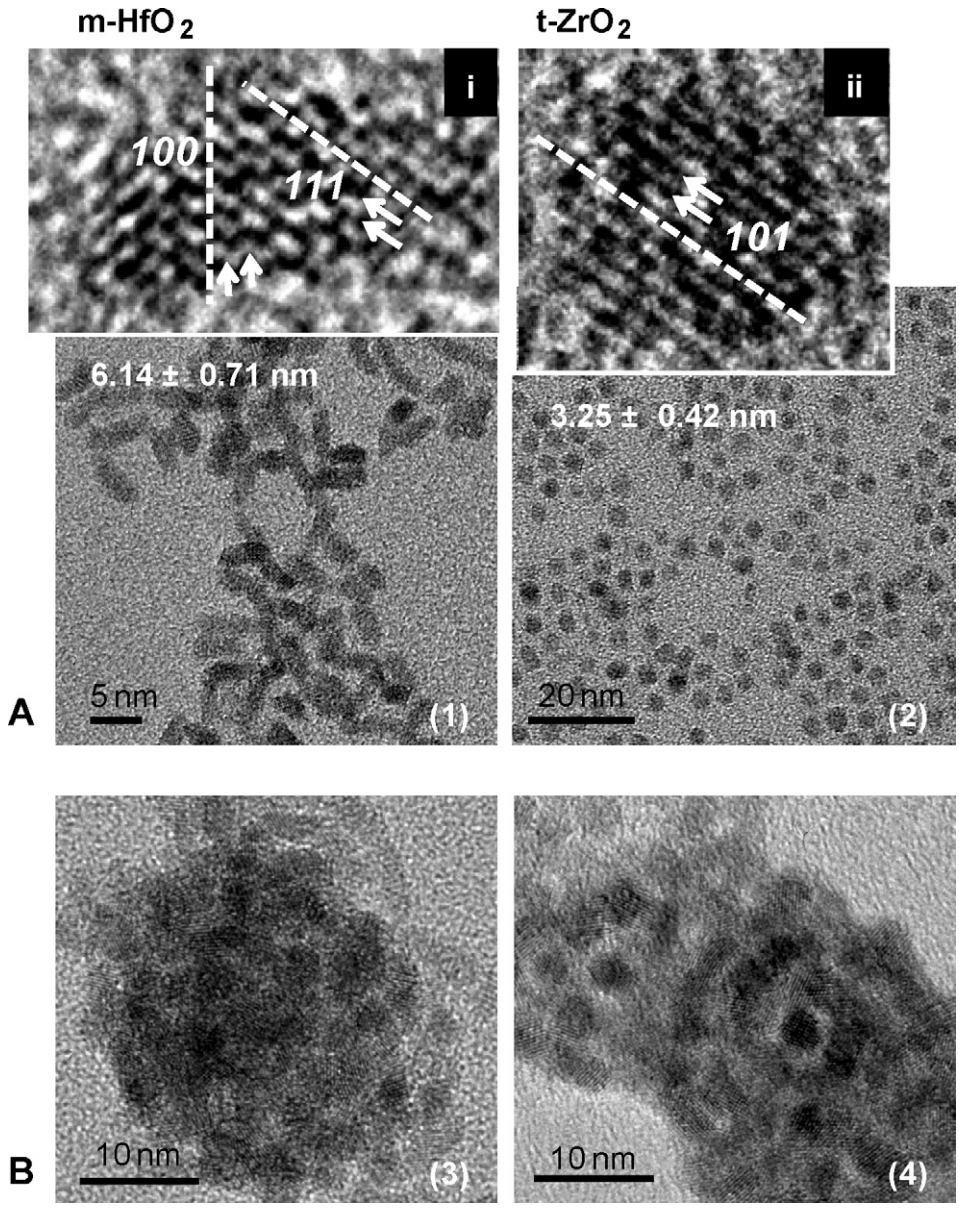

Fig. 1. HRTEM images of (A1–2) the m-HfO_2 and t-ZrO_2 NPs and (B3–4) the HA-transferred MO-NPs in aqueous solution. Insets (i–ii) highlight the predominant crystal planes of the NPs. Lattice spacings were assigned based on monoclinic (JCPDS# 780050) and tetragonal (JCPDS# 881997) structures.

ζ-Potential and DLS data were acquired using a Zetasizer Nano ZS90 instrument (Malvern Instruments, Malvern Hills, UK). TEM measurements were performed using a JEOL JEM-2010 (Tokyo, Japan) operating at an accelerating voltage of 200 kV. Raman spectra were acquired at room temperature using a Horiba Jobin-Yvon (Villeneuve d'Ascq, France) Labram HR Raman spectrometer using 784.51 nm laser excitation from a diode laser. FTIR spectra were collected using a Nicolet-Magna (USA) 550 spectrometer purged with dry air with a spectral resolution of 4 cm^{-1}. Total Hf and Zr concentrations present in the organic and aqueous phase were quantitatively determined by ICP-MS. ICP-MS measurements were conducted using a Thermo Scientific (Germany) X-Series 2 instrument. Concentrations of Hf and/or Zr in the samples were determined using an external calibration curve. Details on sampling and the acid digestion protocol are described in the Supporting information (SI).

3. Results and discussion

3.1. Characteristics of the MO-NPs

Figs. 1A and S1A depicts TEM and lattice-resolved high-resolution TEM (HRTEM) images of m-HfO_2, t-ZrO_2, m-$Hf_{0.37}Zr_{0.67}O_2$, and t-$Hf_{0.37}Zr_{0.67}O_2$ NPs. All NP surfaces are passivated with TOPO and phosphonate ligands. The m-HfO_2 particles adopt an elongated rice-grain-type morphology with aspect ratios ranging from 3 to 4. In contrast, the t-ZrO_2 NPs adopt a quasi-spherical morphology with an average diameter of 3.3 nm. Solid-solution m-$Hf_{0.37}Zr_{0.67}O_2$ NPs are slightly elongated, whereas t-$Hf_{0.37}Zr_{0.67}O_2$ NPs are quasi-spherical [11]. Representative XRD patterns of the MO-NPs used in the phase transfer experiments are shown in Fig. S2. Figs. 1A and S1A demonstrate the monodispersity of the NPs used. The HRTEM images indicate

the exposed crystal facets for each set of particles. The monoclinic NPs consistently show a preference for {1 0 0} and {1 1 1} crystal facets, whereas the tetragonal NPs predominantly exhibit {1 0 1} surface-terminating planes. These assignments are consistent with surface energy calculations for m-HfO_2 and t-ZrO_2, which indicate preferential energetic stabilization for these planes in the monoclinic and tetragonal crystal structures [34,35].

Given the hydrophobic nature of TOPO, it would be reasonable to expect to first approximation that such NPs will have insignificant dispersibilities or mobilities in the aquatic environment. Indeed, these NPs exhibit very low aqueous solubilities: <0.01 μg/L of Hf and <0.02 μg/L of Zr for the m-HfO_2 and t-ZrO_2 NPs, respectively.

3.2. Phase transfer of MO-NPs

3.2.1. Visual examination

In this study, to probe the interactions of NOM with well-defined MO-NPs, we have vigorously stirred hexane suspensions of the four systems noted above with aqueous solutions of SRHA. As evidenced by the TEM images (Figs. 1B and S1B), some phase transfer of MO-NPs into the aqueous phase is noted for all the systems tested here, although there are some key differences in the magnitude of phase transfer depending on the crystal structure (vide infra). Comparison of TEM images (Figs. 1B/S1B to1A/S1A) clearly indicates the formation of MO-HA agglomerates upon phase transfer to the aqueous phase. The images are consistent with the formation of extended amphiphilic humic structures through associations that are stabilized by dispersive hydrophobic interactions, hydrogen bonding, and intramolecular rearrangements [36]. Despite extensive agglomeration of the MO and HA units, the lattice planes of crystalline MO-NPs enable their identification within the amorphous HA matrix. To first approximation, the sizes of the crystalline cores of the NPs do not appear to be affected but considerable agglomeration of NPs within each colloidal humic entity is evidenced.

Figs. 2 and S3 are digital photographs summarizing the results of the mixing experiments. The top layer is the hexane (organic) phase and the bottom layer is the aqueous phase. Agglomeration of the NPs results in significant visible light scattering, observed as cloudiness/turbidity of the solutions. Clearly, at the start of the experiments, the lower aqueous phase is optically transparent. After 5 days of mixing, appreciable turbidity develops in the aqueous phase for the m-HfO_2 and m-$Hf_{0.37}Zr_{0.63}O_2$ NPs, whereas significantly less turbidity is observed for the tetragonal samples; interfacial accumulation of NPs between the organic and aqueous phases is observed to varying extents for the different NPs. After 15 days of mixing, phase transfer and uniform dispersion of NPs in the aqueous phase are evidently most pronounced for the m-HfO_2 and m-$Hf_{0.37}Zr_{0.63}O_2$ samples with the top organic layer almost completely clear. Some interfacial accumulation and phase transfer are observed for the m-HfO_2 and m-$Hf_{0.37}Zr_{0.63}O_2$ NPs even without the addition of HA. However, in the presence of HA, the coated MO-NPs exhibit greater colloidal dispersion and stability with respect to agglomeration upon phase transfer, whereas in the absence of HA, interfacial accumulation appears to dominate and even the particles that are phase transferred to the aqueous phase eventually flocculate from suspension. In stark contrast, the t-ZrO_2 and t-$Hf_{0.37}Zr_{0.63}O_2$ NPs show a significantly lower tendency for phase transfer.

3.2.2. Quantitation by measurement of Hf/Zr concentrations

ICP-MS measurements provide a more quantitative perspective of the colloidal stabilization of the MO-NPs achieved in the aqueous phase. Herein, our goal has been to demonstrate the gradual increase in the concentration of NPs (based on Hf/Zr concentrations) dispersed in the aqueous phase and to compare the extent of phase transfer for monoclinic vs. tetragonal NPs. Hf and Zr concentrations in the organic and aqueous phases (Table 1 and Figs. 3 and S4) show the transfer characteristics of the different MO-NPs over a 15-day period. As also suggested by Figs. 2 and S3, the data show pronounced differences between the phase transfer of monoclinic and tetragonal NPs and similarities between phase transfer in H_2O and in HA. After mixing for 15 days with or without HA, the organic phase appears to be almost completely depleted of m-HfO_2 NPs. The high $HfO_{2(aq.)}/HfO_{2(org.)}$ ratio (Table 1) and the high levels of Hf found in the aqueous phase (~260 mg/L in H_2O and ~280 mg/L in HA) indicate that the m-HfO_2 NPs are significantly partitioned into the aqueous phase. In contrast, very little phase transfer appears to have occurred for the t-ZrO_2 NPs with or without HA, which is also manifested in the $ZrO_{2(aq.)}/ZrO_{2(org.)}$ ratio and low levels of Zr

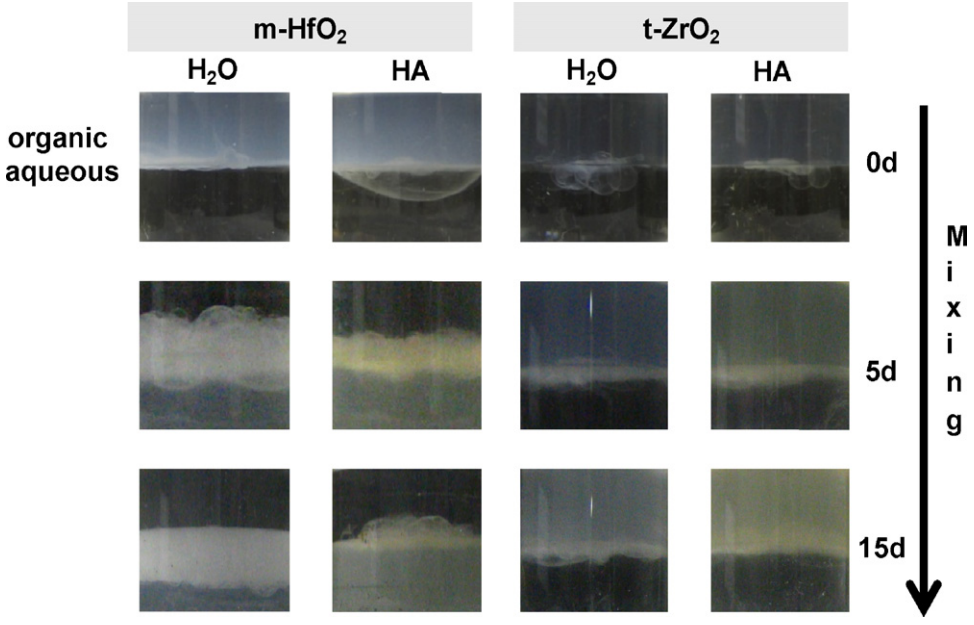

Fig. 2. Digital photographs illustrating phase transfer of the m-HfO_2 and t-ZrO_2 NPs in 20 mg/L HA compared to the control set-ups in H_2O. The top layer is the hexane phase and the bottom layer is the water phase. Similar images for $Hf_{0.37}Zr_{0.63}O_2$ NPs are in Fig. S3.

Table 1
Quantitative information on the phase transfer of the different NPs in 20 mg/L HA and H_2O (control) after 15 days. Ratio of NP concentration in the aqueous and organic phase is determined from the concentration of Hf/Zr in each phase, as measured by ICP-MS.

MO sample	Distribution ratio (D_{iao})[a]	
	H_2O	HA
HfO_2,	61	67
ZrO_2	0.10	0.13
Monoclinic $Hf_{0.37}Zr_{0.63}O_2$[b]	17, 16	5.4, 5.5
Tetragonal $Hf_{0.37}Zr_{0.63}O_2$[b]	0.02, 0.02	0.02, 0.02

[a] D_{iao} = [MO nanocrystal]$_{aqueous}$/[MO nanocrystal]$_{organic}$ = [Hf or Zr]$_{aqueous}$/[Hf or Zr]$_{organic}$.
[b] D_{iao} are reported as ratios calculated from Hf, Zr.

found in the aqueous phase (~5 mg/L Zr in H_2O and HA). To determine whether the observed selectivity of phase transfer arises from differences in chemical composition (m-HfO_2 vs. t-ZrO_2) or crystal structure (monoclinic vs. tetragonal), the same experiments have been performed for solid-solution $Hf_{0.37}Zr_{0.63}O_2$ NPs with identical composition but different crystal structures. It is evident from the results summarized in Table 1, Figs. 3 and S4 that the crystal structure (and not composition) has the predominant effect on the observed phase transfer: significant phase transfer is observed for m-$Hf_{0.37}Zr_{0.63}O_2$ but not t-$Hf_{0.37}Zr_{0.63}O_2$ NPs (analogous to the differences noted above for m-HfO_2 and t-ZrO_2 NPs). After the 15-day period, m-$Hf_{0.37}Zr_{0.63}O_2$ NPs had higher distribution ratios than the t-$Hf_{0.37}Zr_{0.63}O_2$ NPs (Table 1). Levels of Hf (and Zr) were also higher in the aqueous phases of the m-$Hf_{0.37}Zr_{0.63}O_2$ NPs (~150 mg/L Hf in H_2O and ~130 mg/L Hf in HA) than the t-$Hf_{0.37}Zr_{0.63}O_2$ NPs (~4 mg/L Hf in H_2O and ~1 mg/L Hf in HA). It is also interesting that the D_{iao} calculated using concentrations from Hf and Zr correlated well with each other (Table 1) suggesting that intact NPs were transferred. Some differences in the phase-transfer behavior of m-HfO_2 and m-$Hf_{0.37}Zr_{0.63}O_2$ are also apparent in Fig. 3. The m-HfO_2 NPs reached equilibrium within 1 day of mixing, whereas the m-$Hf_{0.37}Zr_{0.63}O_2$ NPs reached equilibrium only after 10 days of mixing; the value of D_{iao} is also higher for m-HfO_2 NPs. Taken together, this set of data implies the primary importance of crystal structure but also shows some distinctions based on the specific Hf content in the NPs.

3.3. Characterization of the phase-transferred MO-NPs

3.3.1. Crystal structure

Fig. 4 shows Raman spectra of the as-prepared colloidal m-HfO_2 NPs along with spectra for solid samples freeze-dried after transfer to the aqueous phase with or without the presence of HA. Notably, the spectrum for the phase-transferred m-HfO_2-HA adducts bears

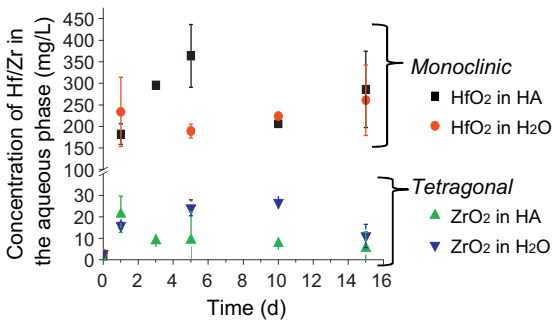

Fig. 3. Concentration vs time plots for the phase transfer of m-HfO_2 and t-ZrO_2 NPs in 20 mg/L HA and in H_2O. Similar plots for $Hf_{0.37}Zr_{0.63}O_2$ NPs are in Fig. S4. Error bars correspond to standard deviation of concentrations determined from different sample aliquots (n = 2).

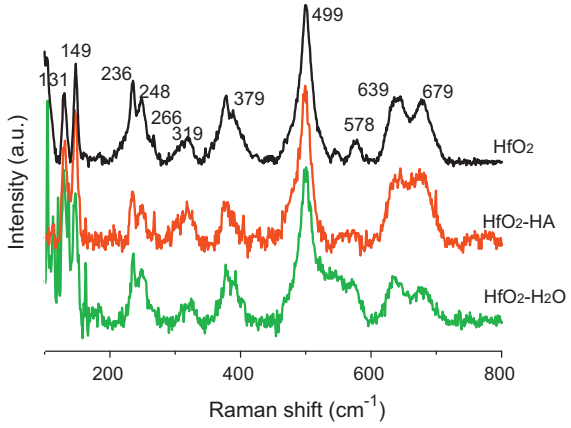

Fig. 4. Raman spectra for as-prepared TOPO-coated m-HfO_2 NPs and phase-transferred HfO_2 NPs transferred in the presence or absence of HA showing the 100–800 cm^{-1} region highlighting the different Raman modes characteristic of monoclinic HfO_2 NPs.

close similarity to the spectrum of the pure NPs. The spectra show characteristic signatures of the monoclinic phase with 14 of the 18 predicted Raman phonon modes for m-HfO_2 clearly identifiable in the 100–800 cm^{-1} range [25]. In other words, the Raman spectra suggest retention of the monoclinic phase even after phase transfer; this data further corroborates TEM evidence that there is no discernible surface reconstruction or change in crystal structure. While some leaching of Hf/Zr ions cannot be ruled out, from the Raman data, there is no evidence for the speciation of other solid phases such as metal hydroxides and phosphates.

3.3.2. Surface charge

A comparison of the ζ-potential distributions for the MO-NPs, HA solution and phase-transferred samples is shown in Figs. 5 and S5. In general, the as-prepared NPs in hexane have broad ζ-potential distributions (positive to negative), whereas HA in water has an overall negative ζ-potential (centered at −20.4 mV). The presence of both positive and negative particles is consistent with hot colloidal syntheses where coordinatively unsaturated cationic and anionic sites are remnant on the NP surface (based on sterics alone, TOPO can not passivate every cationic and anionic site) [41].

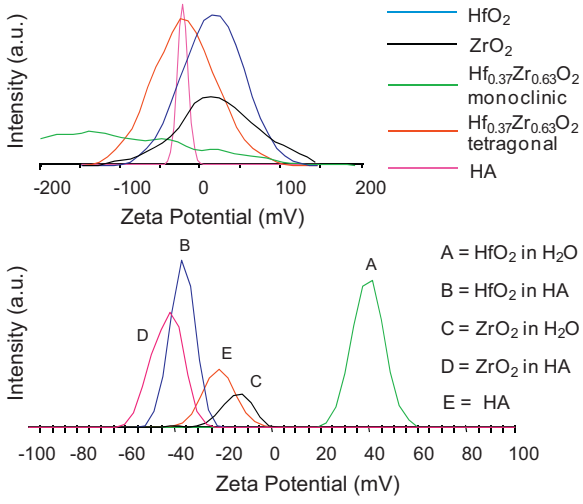

Fig. 5. ζ-Potential distribution of (A) all starting materials, as-prepared TOPO-coated MO-NPs and 20 mg/L HA, and (B) the aqueous phases of the different set-ups after 1 day of continuous mixing. All samples were measured in water except for the NP suspensions which were in hexane. ζ-Potential distribution is from the average of n = 3 measurements.

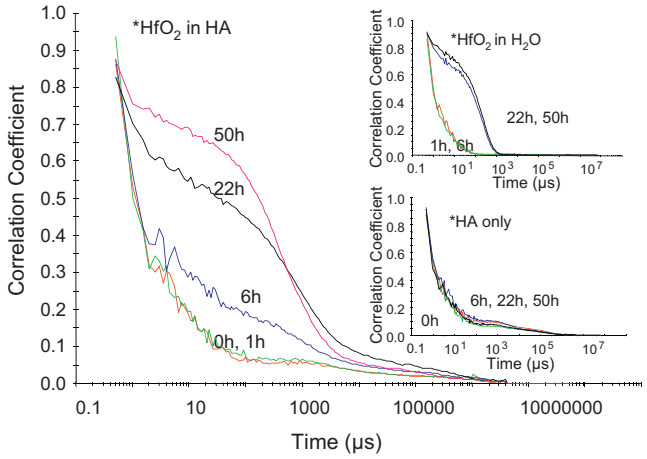

Fig. 6. DLS correlation data (aqueous phase) collected for the phase transfer of m-HfO_2 NPs in 20 mg/L HA. Insets show raw correlation data for the control and as-prepared HA. Correlation data for other MO NPs are in Fig. S4.

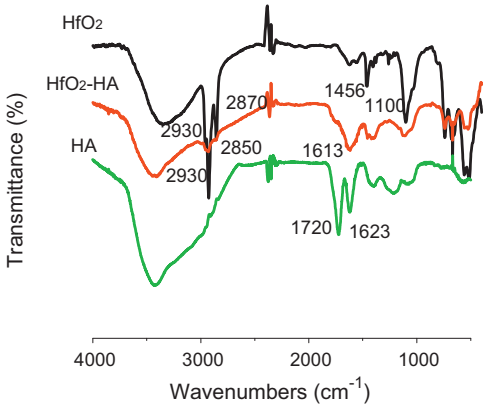

Fig. 7. FTIR spectra of as-prepared TOPO-coated m-HfO_2 NPs, phase-transferred MO-NPs and HA showing the 4000–400 cm^{-1} region.

Nonetheless, the resulting NPs are still considered hydrophobic because of the capping TOPO ligands with their pendant hydrocarbon chains, which are strongly hydrophobic and preclude ready access of other species to charged sites [37]. When the NPs are mixed with HA for 1 day, the ζ-potential values in the aqueous phase shifted to more negative values; from −20.4 mV to −36.8 mV (for m-HfO_2 in HA) and −43.1 mV (for t-ZrO_2 in HA), consistent with other studies [16,17,19]. These values are consistent with the formation of larger, more stable (more negative) HA agglomerates in suspension, as also seen in Fig. 1B. For the MO-HA adducts observed in the TEM, the negative ζ-potential also confirms that the negatively charged humics are present at the surface and envelope the NPs. The shift to more negative ζ-potential values in the presence of HA and the loss of positively charged NPs suggest electrostatic interactions between the two species. Although both m-HfO_2 and t-ZrO_2 experienced the same changes in average ζ-potential, ICP-MS results still show that monoclinic NPs have a stronger predilection to phase transfer compared to tetragonal NPs.

3.3.3. Particle agglomeration

Agglomeration of the NPs during phase transfer has been further monitored by DLS, as shown in Figs. 6, S6 and S7. Fig. 6 compares the DLS correlation curves acquired at different time intervals (0–50 h). As we have noted in a previous research article, the validity of fitting correlograms measured from fixed-angle DLS measurements to extract exponential decays and an "average" size for systems as heterogeneous and polydisperse as MO-HA agglomerates is questionable [30,31]. Consequently, a more reliable and realistic approach involves qualitatively comparing the directly measured correlograms. The shift of the correlograms to longer times implies that the particles stay correlated over longer periods while undergoing Brownian motion—suggesting the formation of larger more sluggish agglomerates. The measured correlation curves for the aqueous phase after mixing m-HfO_2 NPs in hexane with HA for different periods of time are shown in Fig. 6. It is apparent that as the m-HfO_2 NPs transfer from hexane to the aqueous phase, larger species (likely MO-HA agglomerates) are formed. With progressively increased transfer of NPs to the aqueous phase, the MO-HA agglomerates tend to expand in size. The MO-HA adducts first appear in the aqueous phase as early as 6 h after initiation of mixing and subsequently increase in size after 22 and 50 h, as evidenced by the correlation curves; the considerable breadth of the decay traces is indicative of substantial polydispersity in the size of the agglomerates, as also evidenced by the TEM images in Fig. 1B. For the control sample (m-HfO_2 NPs in H_2O), no evidence of adducts is observed before 22 h. Hence, HA considerably accelerates phase transfer in addition to better dispersing the m-HfO_2 NPs in the aqueous phase. DLS data presented in the inset also demonstrate that substantial agglomeration of HA does not occur under these conditions confirming that the observed increase in the times for the correlation curves to decay to the baseline must arise from the transfer of m-HfO_2 NPs to the aqueous phase. Similar results are obtained for the m-$Hf_{0.37}Zr_{0.63}O_2$ NPs (Fig. S6). For the tetragonal NPs exhibiting minimal phase transfer, the DLS correlation curves are shown in Fig. S7. DLS data are unable to pinpoint the specific interactions between HA and MO-NPs that induce phase transfer but clearly establish the role of the HA in this process and are consistent with the formation of MO-HA adducts. Note that although HA provides some extent of colloidal stabilization to the monoclinic NPs, it is a much bulkier molecule that is prone to crosslinking and does not have the steric or electrostatic properties required to completely preclude NP agglomeration over an extended period of time (>2 weeks).

3.3.4. Surface chemistry

To further investigate the nature of the interactions between HA and the MO-NPs, FTIR spectroscopy data for the phase-transferred MO-HA adducts are compared to the data for the individual constituents (Fig. 7). The infrared spectrum of the as-prepared m-HfO_2 NPs is dominated by absorptions that can be attributed to the TOPO ligands. In particular, a strong P=O stretch is observed at 1100 cm^{-1} and asymmetric and symmetric C–H stretches arising from the alkyl groups are observed at ~2850–2930 cm^{-1} [11]. In contrast, HA shows a characteristic O–H band at ~3450 cm^{-1} and asymmetric COO stretches at 1720 cm^{-1} and 1623 cm^{-1} [18,38,39].

FTIR spectra of m-HfO_2-HA adducts recovered from the aqueous phase clearly indicate some peaks characteristic of TOPO, specifically C–H stretching bands at 2930 cm^{-1} and 2850 cm^{-1} as well as the P=O stretching band at ~1100 cm^{-1}, though these are significantly diminished relative to the corresponding peaks for TOPO-coated NPs. The presence of these bands indicates that the TOPO ligands on the NP surfaces are not completely displaced by the functional groups on HA (or by H_2O molecules). Since TOPO has a very low aqueous solubility (0.058 mg/L in H_2O at 25 °C [40]), our results suggest that HA has enabled the phase transfer and aqueous stabilization of the TOPO-coated MO-NPs.

Some peaks characteristic of HA are also apparent in the FTIR spectra for the m-HfO_2-HA adducts, specifically the asymmetric COO stretching bands. In the spectrum acquired for pure HA, prominent asymmetric COO stretches, corresponding to carboxylic acid ($\nu_{as}(CO_2H)$) and carboxylate ($\nu_{as}(CO_2^-)$) moieties [30,31,39], are present at relatively equal intensities. In the spectrum of the

m-HfO_2-HA adducts, there is a significant diminution in the intensity of the ($\nu_{as}(CO_2H)$) band at 1720 cm^{-1} and instead a single prominent $\nu_{as}(CO_2^-)$ band is observed at 1613 cm^{-1}. This shift to lower wavenumbers and dimunition of the $\nu_{as}(CO_2H)$ peak can be attributed to the formation of metal-carboxylate linkages. The precise coordination mode (i.e., monodentate, bidentate) however, cannot be clearly determined since the symmetric carboxylate stretching bands are not adequately well resolved. Although studies of metal-humate complexes with higher valent metal ions are limited, the binding of HA to hafnium has indeed been demonstrated [44].

3.4. Proposed phase transfer mechanism

Taken together, the data presented above provide a clear picture of multiple interfacial interactions that enable the phase transfer and aqueous dispersal of monoclinic MO-NPs. As noted previously for the NOM-induced phase transfer of CdSe quantum dots [30,31], two distinct stages can be demarcated: (1) the flocculation of the MO-NPs at the hexane/water interface wherein a turbid interfacial layer is formed and a large density of surface sites are primed for interactions with H_2O or HA, and (2) dispersion of the NPs from the interface into the aqueous layer where they form a colloidal dispersion that is stable over >2 weeks. In the absence of HA, phase transfer occurs at a relatively slower rate and the transferred MO-NPs tend to flocculate and eventually settle at the bottom of the vial.

Indeed, the TEM images, ζ-potential, DLS, and FTIR spectral data all suggest direct interaction between the MO-NPs and HA. Three distinctive interactions of HA with the MO-NPs leading to aqueous phase dispersal and stabilization can be envisaged [30,31,45]. The first process involves overcoating of the MO-NPs with HA through non-specific adsorption of humics onto the TOPO ligand shell. The amphiphilic characteristics of HA enable the formation of pseudo-micellar agglomerates that overcoat the NPs, wherein hydrophobic aromatic and heteroaliphatic regions form a hydrophobic interior cavity, whereas pendant hydrophilic carboxylic acid, phenolic, and amine moieties are directed outwards imparting colloidal stability in water via electrostatic stabilization [38,46]. Provided that the NP surface ligands are engaged in this interaction, this mechanism is not expected to show any discrimination between monoclinic and tetragonal crystal structures. The second process involves dative interactions between HA and the MO surfaces, where the carboxylic acid (estimated to be 10% in SRHA-II, [47]), phenolic, and amine moieties that are abundant in the HA structure serve as versatile polydentate chelating ligands [38,48–51]. Interaction involving the NP surface is conceivable given the highly reactive surfaces of nanoscale materials, wherein most of the constituent atoms reside at or near the surface [27,28,52]. This mechanism is predicated on the availability and accessibility of metal sites on the MO-NP surface that can participate in coordinative interactions. Different crystal structures have distinctive planes, corners, and edges exposed at the surface (Fig. 1). Hence, in contrast to the overcoating mechanism, this interaction can possibly provide some discrimination between monoclinic and tetragonal crystal structures. The third process involves electrostatic interactions between the coordinatively unsaturated surface sites on the MO-NPs (positively and negatively charged) and the carboxylic and phenolic moieties (negatively charged) in the HA structure.

All these processes (micellar/overcoating, coordinative/substitutional, and electrostatic interactions) appear to work synergistically to facilitate the phase transfer and subsequent aqueous-phase dispersal of monoclinic MO-NPs passivated with TOPO but not the tetragonal NPs. The differences in the phase transfer behavior observed between the two different polymorphs suggest that specific rather than non-specific interactions mediate phase transfer; in this case, the surface-structure-dependent coordinative/subsitutional interactions are the likely genesis of the distinctive reactivity. Upon mixing with H_2O/HA, some of the TOPO ligands are likely displaced; FTIR spectra of phase-transferred MO-HA agglomerates suggest that the amount of TOPO is diminished compared to the TOPO-coated NPs. Removal of TOPO provides access to oxophilic, coordinatively unsaturated cationic sites on the MO-NP surfaces that can be accessed by the carboxylic acid moieties of HA (electrostatic interactions likely induce the initial approach of the HA moieties and NPs). Apart from ligand displacement, incomplete coverage/passivation of the initial NPs by TOPO would also make Hf/Zr surface sites available for binding to HA. Impurities in technical grade TOPO (90%), particularly alkylphosphonic and alkylphosphinic acids that have been shown to play an active role in passivating surfaces of CdSe quantum dots, rods, and wires [53–56], could also influence the interactions between HA and the NP surface [31]. The fractional surface coverage of the coating groups and the precise nature of the ligand passivation shell are beyond the scope of this study (ligand passivation shells remain to be adequately characterized even for CdSe quantum dots that are possibly the most mature of this class of materials). Nonetheless, as suggested by FTIR, the formation of metal–humate linkages tethers the MO-NPs to the humic colloids, which likely draws the NPs to the hexane/water interface such that both the hydrophobic NPs and the hydrophilic HA colloids can be adequately solvated. Subsequently, as described in the literature [46,49,57], the flexible humic colloid can undergo molecular rearrangement and cross-linking with proximal HA moieties at the hexane/water interface to optimize hydrophobic interactions with the pendant aliphatic chains on the TOPO ligand [41–43,58]. In addition, our results indicate that H_2O by itself enables some phase transfer of NPs. The oxophilicity of early transition metal oxide surfaces may also allow for facile ligand substitution by H_2O, which can eventually result in appreciable hydroxylation of the MO surfaces. The affinities of different crystallographic facets for HA may reasonably be assumed to parallel the likelihood of ligand substitution by H_2O, which may explain the significant phase transfer observed for the monoclinic NPs even in the absence of HA. Phase transfer only shows differences between H_2O and HA on shorter timescales, when the MO-H_2O interaction is likely limited by ligand substitution. The interfacial turbidity and shorter-lived phase transfer noted in control samples in the absence of HA likely arise from the displacement of some TOPO ligands by H_2O. Consistent with the proposed mechanism, since surface-coordinated H_2O molecules lack the amphiphilic characteristics of HA, they are not able to adequately stabilize the TOPO-coated MO-NPs in the aqueous phase. In other words, ligand substitution of TOPO by H_2O can induce sedimentation at the hexane/water interface but does not permit colloidal stabilization in the aqueous phase in the absence of HA.

Preferential binding of HA or H_2O to monoclinic instead of tetragonal surfaces may form the basis for the observed selectivity of phase transfer such as between m-HfO_2 and t-ZrO_2 NPs, and between m-$Hf_{0.37}Zr_{0.63}O_2$ and t-$Hf_{0.37}Zr_{0.63}O_2$. As shown in Fig. 1A, the m-HfO_2 (and m-$Hf_{0.37}Zr_{0.63}O_2$) NPs preferentially expose {1 0 0} and {1 1 1} surfaces, whereas for t-ZrO_2 (and t-$Hf_{0.37}Zr_{0.63}O_2$) NPs {1 0 1} surfaces are energetically preferred. While the difference between m-HfO_2 and t-ZrO_2 NPs with regard to phase transfer could be related to the extent/strength of the Hf-HA bonds vs. the Zr-HA bonds, results from m-$Hf_{0.37}Zr_{0.63}O_2$ and t-$Hf_{0.37}Zr_{0.63}O_2$ NPs (same chemical composition) suggest that phase transfer is more responsive to changes in crystal structure. Consequently, despite both having potentially reactive surfaces, we speculate that the differences in phase transfer of the NPs may originate from (a) the relative binding affinities of the different surfaces in monoclinic and tetragonal NPs for TOPO and HA; (b) the degree of

coordinative unsaturation and steric hindrance for transition metal sites in the different surface planes; and (c) the density of exposed transition metal cation sites. A combination of these factors could make metal sites less available and the displacement of TOPO ligands by HA functionalities more difficult for tetragonal NPs. In the absence of metal–humate linkages, phase transfer may not be as readily initiated resulting in the poor phase transfer efficiencies observed for t-ZrO_2 and t-$Hf_{0.37}Zr_{0.63}O_2$ NPs. An analogous preference for binding different surfaces is also expected for coordinative interactions with H_2O molecules. Calculation of binding affinities, extent of surface unsaturation, and density of cation and anions on the NP surface is beyond the scope of this study; these measurements have indeed not been experimentally validated for ligand-passivated colloidal NP systems with any degree of accuracy. Nonetheless, our extensive characterization data is adequate to draw some conclusions with regard to the mechanisms that dictate phase transfer and aqueous phase stabilization of these NPs.

4. Conclusions

The interactions between HA and MO-NPs indicate the role of HA as both a coordinating ligand and an amphiphilic surfactant. Our results further provide experimental validation of theoretical predictions [14] and experimental observations [15–17] of modifications to the colloidal stability of MO-NPs upon the acquisition of NOM coatings. In this study, HA and H_2O both exhibit a distinct preference for monoclinic rather than tetragonal MO-NPs, possibly because of stronger binding affinities to monoclinic surfaces (coordinative/substitutional interactions) and the ease of formation of cylindrical pseudo-micellar structures (overcoating/micellar interaction). The extent of phase transfer and degree of colloidal stabilization observed for well-defined MO-NPs with hydrophobic coatings in the presence of HA also underline the importance of developing a detailed understanding of the potential environmental transformations of ENPs. The distinctive selectivity in the HA-induced phase transfer and dispersion of different polymorphs suggests that interactions of different inorganic ENMs with NOM, which dictate the extent of NP transport and stabilization, are not necessarily generalizable and that it may be possible to design NMs to minimize their residence time in the aquatic environment. In this regard, further research is required to determine the actual binding affinities of HA onto monoclinic and tetragonal surfaces and to investigate the influence of different surface coatings.

Acknowledgements

This work was primarily supported by the US Environmental Protection Agency (Grant# R833861). SB acknowledges partial support of this work from National Science Foundation under DMR 0847169. We acknowledge the NSF MRI Program CHE 0959565 for acquisition of the ICP-MS instrument. Both CSIRO and the US EPA have not subjected this manuscript to internal peer and policy review. Therefore, no official endorsement should be inferred.

Appendix A. Supplementary data

Supplementary data associated with this article can be found, in the online version, at doi:10.1016/j.jhazmat.2011.09.028.

References

[1] P.J.J. Alvarez, V.L. Colvin, J. Lead, V. Stone, Research priorities to advance eco-responsible nanotechnology, ACS Nano 3 (2009) 1616–1619.
[2] A. Maynard, R.J. Aitken, T. Butz, V. Colvin, K. Donaldson, G. Oberdorster, M.A. Philbert, J. Ryan, A. Seaton, V. Stone, S.S. Tinkle, L. Tran, N.J. Walker, D.B. Warheit, Safe handling of nanotechnology, Nature 444 (2006) 267–269.
[3] M.R. Wiesner, G.V. Lowry, P. Alvarez, D. Dionysiou, P. Biswas, Assessing the risks of manufactured nanomaterials, Environ. Sci. Technol. 40 (2006), 4336–4335.
[4] J.R. Peralta-Videa, L.J. Zhao, M.L. Lopez-Moreno, G. de la Rosa, J. Hong, J.L. Gardea-Torresdey, Nanomaterials and the environment: a review for the biennium 2008–2010, J. Hazard. Mater. 186 (2011) 1–15.
[5] E. Casals, S. Vazquez-Campos, N.G. Bastus, V. Puntes, Distribution and potential toxicity of engineered inorganic nanoparticles and carbon structures in biological systems, TrAC, Trends Anal. Chem. 27 (2008) 672–684.
[6] S. Harper, C. Usenko, J.E. Hutchison, B.L.S. Maddux, R.L. Tanguay, In vivo biodistribution and toxicity depends on nanomaterial composition, size, surface functionalisation and route of exposure, J. Exp. Nanosci. 3 (2008) 195–206.
[7] L.S. Karlsson, J. Gustafsson, P. Cronholm, L. Moller, Size-dependent toxicity of metal oxide particles: a comparison between nano- and micrometer size, Toxicol. Lett. 188 (2008) 112–118.
[8] M. Farre, K. Gajda-Schrantz, L. Kantiani, D. Barcelo, Ecotoxicity and analysis of nanomaterials in the aquatic environment, Anal. Bioanal. Chem. 393 (2009) 81–95.
[9] A.M.E. Maynard, The Nanotechnology Consumer Products Inventory, Woodrow Wilson International Center for Scholars, The PEW Charitable Trusts, 2006.
[10] A.I. Kingon, J.-P. Maria, S.K. Streiffer, Alternative dielectrics to silicon dioxide for memory and logic devices, Nature (London U. K.) 406 (2000) 1032–1038.
[11] S.W. Depner, K.R. Kort, S. Banerjee, Precursor control of crystal structure and stoichiometry in twin metal oxide nanocrystals, CrystEngComm 11 (2009) 841–846.
[12] A. Facchetti, M.-H. Yoon, T.J. Marks, Gate dielectrics for organic field-effect transistors: new opportunities for organic electronics, Adv. Mater. (Weinheim, Germany) 17 (2005) 1705–1725.
[13] J. Tang, J. Fabbri, R.D. Robinson, Y. Zhu, I.P. Herman, M.L. Steigerwald, L.E. Brus, Solid-solution nanoparticles: use of a nonhydrolytic sol–gel synthesis to prepare HfO_2 and $Hf_xZr_{1-x}O_2$ nanocrystals, Chem. Mater. 16 (2004) 1336–1342.
[14] N.T. Loux, N. Savage, An assessment of the fate of metal oxide nanomaterials in porous media, Water Air Soil Pollut. 194 (2008) 227–241.
[15] S.-W. Bian, I.A. Mudunkotuwa, T. Rupasinghe, V.H. Grassian, Aggregation and dissolution of 4 nm ZnO nanoparticles in aqueous environments: influence of pH, ionic strength, size, and adsorption of humic acid, Langmuir 27 (2011) 6059–6068.
[16] J.D. Hu, Y. Zevi, X.M. Kou, J. Xiao, X.J. Wang, Y. Jin, Effect of dissolved organic matter on the stability of magnetite nanoparticles under different pH and ionic strength conditions, Sci. Total Environ. 408 (2010) 3477–3489.
[17] Y. Zhang, Y.S. Chen, P. Westerhoff, J. Crittenden, Impact of natural organic matter and divalent cations on the stability of aqueous nanoparticles, Water Res. 43 (2009) 4249–4257.
[18] H. Hyung, J.D. Fortner, J.B. Hughes, J.-H. Kim, Natural organic matter stabilizes carbon nanotubes in the aqueous phase, Environ. Sci. Technol. 41 (2007) 179–184.
[19] E. Navarro, A. Baun, R. Behra, N.B. Hartmann, J. Filser, A.-J. Miao, A. Quigg, P.H. Santschi, L. Sigg, Environmental behavior and ecotoxicity of engineered nanoparticles to algae, plants, and fungi, Ecotoxicology 17 (2008) 372–386.
[20] A.A. Keller, H.T. Wang, D.X. Zhou, H.S. Lenihan, G. Cherr, B.J. Cardinale, R. Miller, Z.X. Ji, Stability, Aggregation of metal oxide nanoparticles in natural aqueous matrices, Environ. Sci. Technol. 44 (2010) 1962–1967.
[21] M.F. Benedetti, C.J. Milne, D.G. Kinniburgh, W.H. Van Riemsdijk, L.K. Koopal, Metal ion binding to humic substances: application of the non-ideal competitive adsorption model, Environ. Sci. Technol. 29 (1995) 446–457.
[22] E.M. Perdue, J.H. Reuter, R.S. Parrish, A statistical model of proton binding by humus, Geochim. Cosmochim. Acta 48 (1984) 1257–1263.
[23] D.G. Lumsdon, A.R. Fraser, Infrared spectroscopic evidence supporting heterogeneous site binding models for humic substances, Environ. Sci. Technol. 39 (2005) 6624–6631.
[24] S.W. Depner, K.R. Kort, C. Jaye, D.A. Fischer, S. Banerjee, Nonhydrolytic synthesis and electronic structure of ligand-capped $CeO_{2-\delta}$ and CeOCl nanocrystals, J. Phys. Chem. C 113 (2009) 14126–14134.
[25] R.D. Robinson, J. Tang, M.S. Steigerwald, L.E. Brus, I.P. Herman, Raman scattering in $Hf_xZr_{1-x}O_2$ nanoparticles, Phys. Rev. B Condens. Matter Mater. Phys. 71 (2005) 115408.
[26] D. Schodek, P. Ferreira, M. Ashby, Nanomaterials Nanotechnologies and Design, Elsevier, Burlington, MA, 2009.
[27] I.A. Mudunkotuwa, V.H. Grassian, The devil is in the details (or the surface): impact of surface structure and surface energetics on understanding the behavior of nanomaterials in the environment, J. Environ. Monit. 13 (2011) 1135–1144.
[28] V.H. Grassian, When size really matters: size-dependent properties and surface chemistry of metal and metal oxide nanoparticles in gas and liquid phase environments, J. Phys. Chem. C 112 (2008) 18303–18313.
[29] A.M. Derfus, W.C.W. Chan, S.N. Bhatia, Probing the cytotoxicity of semiconductor quantum dots, Nano Lett. 4 (2004) 11–18.
[30] D.A. Navarro, D.F. Watson, D.S. Aga, S. Banerjee, Natural organic matter-mediated phase transfer of quantum dots in the aquatic environment, Environ. Sci. Technol. 43 (2009) 677–682.
[31] D.A. Navarro, S. Banerjee, D.S. Aga, D.F. Watson, Partitioning of hydrophobic CdSe quantum dots into aqueous dispersions of humic substances: influence of capping-group functionality on the phase-transfer mechanism, J. Colloid Interface Sci. 348 (2010) 119–128.
[32] W.W. Yu, E. Chang, J.C. Falkner, J. Zhang, A.M. Al-Somali, C.M. Sayes, J. Johns, R. Drezek, V.L. Colvin, Forming biocompatible and nonaggregated nanocrystals in water using amphiphilic polymers, J. Am. Chem. Soc. 129 (2007) 2871–2879.

[33] J.A. Leenheer, J.-P. Croué, Characterizing aquatic dissolved organic matter, Environ. Sci. Technol. 37 (2003) 18A–26A.
[34] I.M. Iskandarova, A.A. Knizhnik, E.A. Rykova, A.A. Bagatur'yants, B.V. Potapkin, A.A. Korkin, First-principle investigation of the hydroxylation of zirconia and hafnia surfaces, Microelectron. Eng. 69 (2003) 587–593.
[35] A.B. Mukhopadhyay, J.F. Sanz, C.B. Musgrave, First-principles calculations of structural and electronic properties of monoclinic hafnia surfaces, Phys. Rev. B Condens. Matter Mater. Phys. 73 (2006) 115330.
[36] F.R. Rizzi, S. Stoll, N. Senesi, J. Buffle, A transmission electron microscopy study of the fractal properties and aggregation processes of humic acids, Soil Sci. 169 (2004) 765–775.
[37] S. Jia, S. Banerjee, I.P. Herman, Mechanism of the electrophoretic deposition of CdSe nanocrystal films: influence of the nanocrystal surface and charge, J. Phys. Chem. C 112 (2008) 162–171.
[38] B. Sutton, G. Sposito, Molecular structure in soil humic substances: the new view, Environ. Sci. Technol. 39 (2005) 9009–9015.
[39] K.M. Elkins, D.J. Nelson, Spectroscopic approaches to the study of the interaction of aluminum with humic substances, Coord. Chem. Rev. 228 (2002) 205–225.
[40] SciFinder Scholar Substance Identifier as calculated using Advanced Chemistry Development (ACD/Labs) software V11.02 © 1994–2011, in.
[41] C.T. Chiou, D.E. Kile, T.I. Brinton, R.L. Malcolm, J.A. Leenheer, P. MacCarthy, A comparison of water solubility enhancements of organic solutes by aquatic humic materials and commercial humic acids, Environ. Sci. Technol. 21 (1987) 1231–1234.
[42] H.-H. Cho, J.-W. Park, C.C.K. Liu, Effect of molecular structures on the solubility enhancement of hydrophobic organic compounds by environmental amphiphiles, Environ. Toxicol. Chem. 21 (2002) 999–1003.
[43] D.E. Kile, C.T. Chiou, Water solubility enhancements of DDT and trichlorobenzene by some surfactants below and above the critical micelle concentration, Environ. Sci. Technol. 23 (1989) 832–838.
[44] N. Rawat, S. Kumar, B. Tomar, The time differential perturbed angular correlation study of binding of hafnium to humic acid and its model compound, Polyhedron 28 (2009) 1399–1402.
[45] S. Diegoli, A.L. Manciulea, S. Begum, I.P. Jones, J.R. Lead, J.A. Preece, Interaction between manufactured gold nanoparticles and naturally occurring organic macromolecules, Sci. Total Environ. 402 (2008) 51–61.
[46] R.L. Wershaw, A new model for humic materials and their interactions with hydrophobic organic chemicals in soil–water or sediment–water systems, J. Contam. Hydrol. 1 (1986) 29–45.
[47] 13C NMR Estimates of Carbon Distribution in IHSS Samples, in, International Humic Substances Society.
[48] M. Baalousha, M. Montelica-Heino, P. Le Coustumer, Conformation and size of humic substances: effects of major cation concentration and type pH, salinity, and residence time, Colloids Surf. A 272 (2006) 48–55.
[49] C.E. Clapp, M.H.B. Hayes, Sizes and shapes of humic substances, Soil Sci. 164 (1999) 777–789.
[50] M. Schnitzer, S.I.M. Skinner, Organometallic interactions in soils. III. Properties of iron- and aluminum-organic matter complexes prepared in the laboratory and extracted from a soil, Soil Sci. 98 (1964) 197–203.
[51] M. Schnitzer, S.I.M. Skinner, Organo metallic interactions in soils. IV. Carboxyl and hydroxyl groups in organic matter and metal retention, Soil Sci. 99 (1965) 278–284.
[52] C. Burda, X. Chen, R. Narayanan, M.A. El-Sayed, Chemistry and properties of nanocrystals of different shapes, Chem. Rev. (Washington DC, United States) 105 (2005) 1025–1102.
[53] J.T. Kopping, T.E. Patten, Identification of acidic phosphorus-containing ligands involved in the surface chemistry of CdSe nanoparticles prepared in tri-*n*-octylphosphine oxide solvents, J. Am. Chem. Soc. 130 (2008) 5689–5698.
[54] F. Wang, R. Tang, W.E. Buhro, The trouble with TOPO; identification of adventitious impurities beneficial to the growth of cadmium selenide quamtum dots, rods, and wires, Nano Lett. 8 (2008) 3521–3524.
[55] F. Wang, R. Tang, J.L.-F. Kao, S.D. Dingman, W.E. Buhro, Spectroscopic identification of tri-*n*-octylphosphine oxide (TOPO) impurities and elucidation of their roles in cadmium selenide quantum-wire growth, J. Am. Chem. Soc. 131 (2009) 4983–4994.
[56] J.S. Owen, J. Park, P.-E. Trudeau, A.P. Alivisatos, Reaction chemistry and ligand exchange at cadmium–selenide nanocrystal surfaces, J. Am. Chem. Soc. 130 (2008) 12279–12281.
[57] L.T. Sein, J.M. Varnum, S.A. Jansen, Conformational modeling of a new building block of humic acid: approaches to the lowest energy conformer, Environ. Sci. Technol. 33 (1999) 546–552.
[58] Y. Lu, J.J. Pignatello, Sorption of apolar aromatic compounds to soil humic acid particles affected by aluminum(III) ion crosslinking, J. Environ. Qual. 33 (2004) 1314–1321.